Applied Catalysis A: General 491 (2015) 58–69

Contents lists available at ScienceDirect

Applied Catalysis A: General

journal homepage: www.elsevier.com/locate/apcata

Highly efficient and magnetically recyclable graphene-supported Pd/Fe_3O_4 nanoparticle catalysts for Suzuki and Heck cross-coupling reactions

Hany A. Elazab[b], Ali R. Siamaki[b], Sherif Moussa[a], B. Frank Gupton[a,b,*], M. Samy El-Shall[a,b,c,*]

[a] Department of Chemistry, Virginia Commonwealth University, Richmond, VA, 23284
[b] Department of Chemical Engineering, Virginia Commonwealth University, Richmond, VA, 23284
[c] Department of Chemistry, Faculty of Science, King Abdulaziz University, Jeddah 21589, Saudi Arabia

ARTICLE INFO

Article history:
Received 31 July 2014
Received in revised form
11 November 2014
Accepted 18 November 2014
Available online 26 November 2014

Keywords:
Magnetite nanoparticles
Palladium/magnetite/graphene catalyst
Suzuki coupling
Heck coupling
Magnetic separation of catalysts

ABSTRACT

Herein, we report a facile and efficient one-step method for the synthesis of highly active, Pd/Fe_3O_4 nanoparticles supported on graphene nanosheets ($Pd/Fe_3O_4/G$) that exhibit excellent catalytic activity for Suzuki and Heck coupling reactions and that can be magnetically separated from the reaction mixture and recycled multiple times without loss of catalytic activity. The synthesis approach is based on the Microwave (MW)-assisted reduction of palladium and ferric nitrates in the presence of graphene oxide (GO) nanosheets using hydrazine hydrate as the reducing agent. The results provide a fundamental understanding of the system variables by comparing the catalytic activity and recyclability of four different catalysts with different properties. The most active and recyclable catalyst contains 7.6 wt% Pd nanoparticles with 4-6 nm diameters in Pd(0) oxidation state well-dispersed with 30 wt% Fe_3O_4 nanoparticles with 12–16 nm diameters on highly reduced GO containing a C/O ratio of 8.1. These combined properties produce remarkable catalytic activity for Suzuki cross coupling reactions under MW reaction conditions with an extremely high turnover number (TON) of 9250 and turn over frequency (TOF) of 111,000 h^{-1} at 80 °C. The magnetic properties imparted by the Fe_3O_4 component of the catalyst enables the catalyst to be easily isolated and recycled, thus greatly simplifying the ability to purify the reaction products and increasing the economic value of the catalyst. The utility of these magnetic catalysts towards Suzuki and Heck cross coupling reactions with a variety of functionalized substrates was also demonstrated.

1. Introduction

The Suzuki (or the Suzuki-Miyaura) cross-coupling reactions have rapidly become one of the most effective tools in organic synthesis for C—C bond formation and the subsequent assembly of highly functionalized molecules [1–5]. These reactions have been widely used for the assembly of complex organic molecules in a broad range of applications in the chemical and pharmaceutical industries. Cross-coupling reactions have been most frequently carried out under homogeneous conditions employing a ligand to enhance the catalytic activity and selectivity for specific reactions [1,6]. Palladium-based catalysts are considered the most efficient cross-coupling catalysts offering fast reaction rates, high turnover frequency and good selectivity in various synthetic protocols. However, the issues associated with homogeneous catalysis remain a challenge to pharmaceutical applications due to the lack of recyclability and potential contamination from residual metals in the reaction product [6–9]. Ligand-free heterogeneous palladium catalysis presents a promising option to address this problem due to their easy handling, simple recovery, and efficient recycling as evidenced by the significant increase in research efforts in this area [2,3,10–14]. Therefore, the development of highly active heterogeneous Pd nanocatalysts that can be easily separated from the reaction medium and recycled is an important goal of nanomaterials research that is likely to have considerable impact on cross-coupling applications in the future.

Recent attempts to develop highly efficient and recyclable catalysts for cross-coupling reactions have focused on using nanocarbon materials such as carbon nanofibers, carbon nanotubes

* Corresponding authors. Tel.: +1 804 828 3518; fax: +1 804 828 8599.
E-mail addresses: bfgupton@vcu.edu (B.F. Gupton), mselshal@vcu.edu (M.S. El-Shall).

http://dx.doi.org/10.1016/j.apcata.2014.11.033
0926-860X/

(CNTs) and graphene as support systems for the palladium-based catalysts [15–20]. In fact, nanocarbon materials are becoming an emerging area in the development of advanced supported catalysts in general due to their chemical and thermal stability, large surface area, limited interaction with the metal catalysts, and easy recovery of noble metals from the spent catalysts [21,22]. Among the different nanocarbon materials, graphene has shown unique properties and remarkable tunability in supporting a variety of metallic and bimetallic nanoparticle catalysts in heterogeneous catalysis [23–26]. In addition to its unique electronic properties, other properties such as high thermal, chemical, and mechanical stability as well as high surface area (2600 $m^2\ g^{-1}$, theoretical value) also represent desirable characteristics as 2-D support layers for metallic and bimetallic nanoparticles in heterogeneous catalysis [23–26]. Furthermore, structural defects in graphene can be useful as they make it possible to achieve new surface functionalities which enhance the interactions with the anchored metal nanoparticles [27–29]. The defect sites incorporated in the sp^2-bonded carbon network of graphene would provide stability against particle growth to the metal nanoparticle catalysts without inhibiting their activation. Because of the well-defined structure of graphene, it is potentially possible to have controlled types of defects that can be tuned to have the desired catalytic functionalities or surface properties [22]. Furthermore, because of the extended π-system in graphene and its high electron density, it may be easier to reduce metal ions thus generating catalytically active metal centers anchored to the graphene support.

Recently, we reported a remarkable cross-coupling catalytic activity of palladium nanoparticles supported onto graphene nanosheets [18]. The catalyst was prepared from palladium nitrate and graphene oxide (GO) using hydrazine hydrate as a reducing agent under microwave irradiation heating (MWI) [18,26]. This procedure which couples the nucleation of Pd nanoparticles with the reduction of GO, yielded highly uniform palladium nanoparticles evenly distributed across the graphene nanosheets. These catalysts demonstrated extremely high turnover frequencies (108,000 h^{-1}) for Suzuki coupling reactions and were easily recovered and recycled under batch reaction conditions [18]. We also introduced the laser synthesis of Pd nanocatalysts supported on the partially reduced graphene oxide nanosheets (Pd/PRGO) which exhibit excellent catalytic activity for Suzuki, Heck, and Sonogashira cross coupling reactions [19]. These results suggest that the defect sites generated on graphene or on the PRGO nanosheets during the microwave heating or the laser photochemical process could act as favorable nucleation sites for the formation and anchoring of the Pd nanoparticles on the support surface which results in imparting the exceptional catalytic properties to these catalysts.

The most important features of the Pd/graphene and Pd/PRGO catalysts are their very high turnover frequencies for Suzuki cross-coupling reactions (108,000 h^{-1} at 80 °C and 230,000 h^{-1} at 120 °C, respectively) and their ability to be recycled multiple times without loss of catalytic activity [18,19]. However, the isolation of these catalysts from the reaction mixture by conventional filtration methods was found to be quite difficult and time consuming. In order to address this issue, we hypothesized that we could employ the same synthetic strategy of coupling the nucleation and growth of the metal nanoparticles with the reduction of GO to prepare bimetallic Pd-Fe or Pd/Fe_3O_4 nanoparticles supported on graphene, which would provide a means to magnetically separate these catalysts from the reaction mixture [30]. Most of the methods developed for the syntheses of magnetically separable Pd/Fe_3O_4 catalysts involve complex multi-step syntheses not appropriate for economically feasible industrial scale production [31–34]. Herein, we report a facile and highly efficient method for the synthesis of highly active, Pd/Fe_3O_4 nanoparticles supported on graphene nanosheets (Pd/Fe_3O_4/G) that exhibit excellent Suzuki and Heck cross-coupling catalytic activity and can be magnetically separated from the reaction mixture and recycled multiple times without loss of catalytic activity.

In this paper, we introduce a simple and rapid one-step method for the synthesis of Pd-Fe_3O_4 composite nanoparticles supported on graphene. The resulting magnetic catalysts are of prime interest since they combine the high catalytic activity of small Pd nanoparticles and the magnetic properties of Fe_3O_4 nanoparticles that might also enhance the catalytic activity, in addition to being readily collected and recycled with high efficiency. The synthesis approach is based on the MWI - assisted reduction method that we developed for the reduction of GO and for the synthesis of metal nanoparticles supported on graphene [18,20,24,26]. The main advantage of MWI over other conventional heating methods is the rapid and uniform heating of the reaction mixture [35–38]. Due to the difference in the solvent and reactant dielectric constants, selective dielectric heating can provide significant enhancement in the transfer of energy directly to the reactants which causes an instantaneous internal temperature rise [35–38]. This temperature rise in the presence of an appropriate chemical reducing agent allows the simultaneous reduction of the metal ions and GO and the dispersion of the metal nanoparticles on the large surface area of the resulting graphene nanosheets [18,20,24,26]. The non-equilibrium dielectric heating of GO is expected to result in structural defects in the reduced GO sheets. These defect sites, consisting of large vacancies and missing atoms, act as nucleation centers for the Pd-Fe_3O_4 composite nanoparticles which can be anchored to the graphene sheets thus decreasing their mobility under typical reaction conditions and minimizing the potential of their agglomeration and the subsequent decrease in the catalytic activity.

The overall goal of this paper is to introduce a new class of highly active and magnetically recyclable Pd/Fe_3O_4/graphene catalysts and to fundamentally understand the system variables in the application of these catalysts for catalyzing Suzuki and Heck cross-coupling reactions.

2. Experimental

All chemicals were purchased and used as received without further purification. Palladium nitrate (10 wt. % in 10 wt. % HNO_3, 99.999%), hydrazine hydrate (80%, Hydrazine 51%), aryl bromides and chlorides, bromobenzene, and potassium carbonate were obtained from Sigma Aldrich. Deionized water (D.I. H_2O, ~18 MΩ) was used for all experiments. High-purity graphite powder (99.9999%, 200 mesh) was purchased from Alfa Aesar. A mixture of ethanol/deionized water was used for the Suzuki cross-coupling reactions. A JEOL JEM-1230 electron microscope operated at 120 kV and equipped with a Gatan UltraScan 4000SP 4 K × 4 K CCD camera was used to obtain TEM images. TEM samples were prepared by placing a droplet of the prepared catalyst dissolved in ethanol on a 300-mesh copper grid (Ted Pella) which was then left to evaporate in air at room temperature. The X-ray photoelectron spectroscopy (XPS) analysis was performed on a Thermo Fisher Scientific ESCALAB 250 using a monochromatic Al KR X-ray. The X-ray diffraction patterns were measured at room temperature using an X'Pert PRO PANanalytical X-ray diffraction unit. The magnetic properties of the graphene-supported Pd/Fe_3O_4/G catalysts were investigated using a vibrating sample magnetometer (VSM) at room temperature. GC–MS analyses were performed on an Agilent 6890 gas chromatograph equipped with an Agilent 5973 mass selective detector. A CEM Discover microwave instrument was used for cross-coupling reactions. The reactions were performed at operator selectable power output of 250 W.

Table 1
Composition of the Pd/Fe_3O_4 (Catalyst **1**) and the Pd/Fe_3O_4/G Catalysts **2**–**4**.

Catalyst	1	2	3	4
Pd (wt%)[a]	50 (48.5)[a]	20 (18.4)[a]	10 (7.6)[a]	6 (4.8)[a]
$Fe(NO_3)_3.9H_2O$ (wt%)	50	20	30	34
Graphene Oxide (wt%)	–	60	60	60

[a] As determined by ICP-MS.

3. Catalyst preparation

3.1. Synthesis of graphene oxide

GO was prepared according to the Hummers and Offeman method in which oxidation of high-purity graphite powder (99.9999%, 200 mesh) was performed using a mixture of H_2SO_4/$KMnO_4$ [39]. Graphite (4.5 g, 0.375 mol) and $NaNO_3$ (2.5 g, 0.0294 mol) were mixed in a conical flask and the mixture was kept in an ice bath under continuous stirring while slowly adding a solution of concentrated H_2SO_4 (115 ml, 2.157 mol) followed by $KMnO_4$ (15 g, 0.095 mol) over a period of 2.5 h. After addition of deionized water (230 ml) to the above mixture, the temperature of the mixture was kept constant at 80 °C. After 20 min stirring; the second portion of deionized water (700 mL) along with (10%) H_2O_2 (20 mL, 0.667 mol) were added and the mixture was stirred for an additional 5 min. The resulting yellow-brownish cake was washed several times with 1 M HCl (20 mL) followed by hot deionized water (3 L). The resulting GO solid was dried under vacuum at 60 °C overnight. Ultrasonication afforded the exfoliated water dispersed GO solution.

3.2. Synthesis of Pd-Fe_3O_4 supported on graphene

To examine the effects of the support, the loading of Pd nanoparticles, and the oxidation states of Pd (Pd(0) vs. Pd(II)) on the catalytic activity, 15 Pd/Fe_3O_4/G catalysts with different compositions were screened for the Suzuki cross coupling reaction of bromobenzene and phenylboronic acid in a mixture of H_2O:EtOH (1:1). Based on this survey, four catalysts were selected for a comparative detailed study as shown in Table 1 (values listed in brackets). Catalysts **1–4** contain different Pd loadings from the highest Pd content (50 wt% in **Catalyst 1**) to the lowest Pd content (6 wt% in **Catalyst 4**). The actual Pd contents in the four catalysts were measured by ICP-MS analysis as shown in Table 1. Catalyst **1** was selected based on the reactivity of several Pd/Fe_3O_4 catalysts where the highest activity was obtained for the 50 wt% Pd/Fe_3O_4 catalyst. Catalyst **2** was selected to examine the effect of Pd(II) since this catalyst has the highest of Pd(II)/Pd(0) due to inefficient reduction under the preparation conditions described below. This catalyst also includes partially reduced GO. Catalysts **3** contains the highest Pd(0)/Pd(II) ratio and also the highest C/O ratio of 8.1 in the reduced GO. Catalyst **4** has the smallest Pd loading but otherwise nearly similar properties to catalyst **3**.

3.3. Preparation of catalyst *1*

Palladium nitrate (10 wt. % in 10 wt. % HNO_3, 99.999%, 1000 μL) was added to a solution of Fe $(NO_3)_3{\cdot}9H_2O$ (317.5 mg, 0.785 mmol) in 50 mL deionized water and the solution was stirred for 3 hs. Hydrazine hydrate was slowly added as the reducing agent to this mixture at ambient temperature and the solution was further heated under microwave irradiation (1000 W, 2.45 MHz) for 120 s. The final dark black colored solution was filtered and the resulting black solid was washed with hot deionized water (50 mL) 3 times, ethanol (20 mL) 3 times, and then dried in the oven at 80 °C.

The same procedure was used for the preparation of catalysts **2–4** except for the addition of GO and the use of different amounts of reagents as follows:

Catalyst 2: GO (60 mg), $Fe(NO_3)_3{\cdot}9H_2O$ (127 mg, 0.314 mmol), Palladium nitrate (10 wt.% in 10 wt. % HNO_3, 99.999%, 400 μL).
Catalyst 3: GO (60 mg), $Fe(NO_3)_3{\cdot}9H_2O$ (190.5 mg, 0.471 mmol), Palladium nitrate (10 wt.% in 10 wt. % HNO_3, 99.999%, 200 μL).
Catalyst 4: GO (60 mg), $Fe(NO_3)_3{\cdot}9H_2O$ (216 mg, 0.534 mmol), (10 wt. % in 10 wt. % HNO_3, 99.999%, 120 μL).

3.4. General procedure for Suzuki reactions

Aryl bromide (0.32 mmol, 1 eq.) was dissolved in a mixture of 4 mL H_2O:EtOH (1:1) and placed in a 10 mL microwave tube. The aryl boronic acid (0.384 mmol, 1.2 eq.) and potassium carbonate (0.96 mmol, 3 eq.) were added to this mixture. The palladium-Fe_3O_4 supported on graphene nanoparticles (Pd/Fe_3O_4/G) (1.34 mg, 0.96 μmol, 0.3 mol %) was then added, the tube was sealed, and heated under microwave irradiation (250 W, 2.45 MHz) at 80 °C for 10 min. After the reaction was completed, the reaction mixture was extracted with CH_2Cl_2 (3 × 50 mL). The organic layers were combined, dried over anhydrous $MgSO_4$, and filtered. The solvent in the filtrate was removed under vacuum to give a solid product which was further purified by flash chromatography using hexane: ethyl acetate as the eluent.

3.5. General procedure for Heck reactions

Aryl bromide (0.32 mmol, 1 eq.) was dissolved in a mixture of 4 mL H_2O: EtOH (1:1) and placed in a 10 mL microwave tube. To this was added the corresponding alkene (0.64 mmol, 2 eq.) and potassium carbonate (0.96 mmol, 3 eq.). (Pd/Fe_3O_4/G) (1.34 mg, 0.96 μmol, 0.3 mol %) was then added, the tube was sealed, and heated under microwave irradiation (250 W, 2.54 MHz) at 150 °C, for 10 min. Upon the completion of microwave heating, the reaction mixture was extracted with CH_2Cl_2 (3 × 50 mL). The organic layers were combined, dried over anhydrous $MgSO_4$ and filtered. The solvent in the filtrate was then removed under vacuum to give a solid. The pure products were obtained by flash chromatography using hexane:ethyl acetate as eluent.

3.6. General procedure for catalyst recycling

Bromobenzene (50 mg, 0.32 mmol, 1 eq.) was dissolved in a mixture of 4 mL H_2O:EtOH (1:1) and placed in a 10 mL microwave tube. To this was added phenyl boronic acid (47 mg, 0.382 mmol, 1.2 eq.), and potassium carbonate (133 mg, 0.96 mmol, 3 eq.). The Pd-Fe_3O_4 nanoparticles supported on graphene (Pd/Fe_3O_4/G) (2.24 mg, 1.6 μmol, 0.5 mol %) were then added, the tube was sealed, and heated under microwave irradiation (250 W, 2.54 MHz) at 80 °C for 10 min. The progress of the reaction was monitored using GC-MS analysis of an aliquot of the reaction mixture. The reaction mixture was further diluted with ethanol (10 mL) to dissolve the products in the solution and the Pd/Fe_3O_4/G nanoparticles were completely precipitated at the bottom of the tube by means of a strong magnetic field. The ethanol-water solvents were further decanted and the ethanol washing and magnetic precipitation was repeated 2 more times to assure the removal of all the organic materials from the surface of the catalyst. The catalyst was then transferred directly to another microwave tube and fresh reagents were added for the next run. The procedure of recycling the catalyst was repeated for every run, and the GC-MS spectroscopy was used to determine the percent conversion of the product.

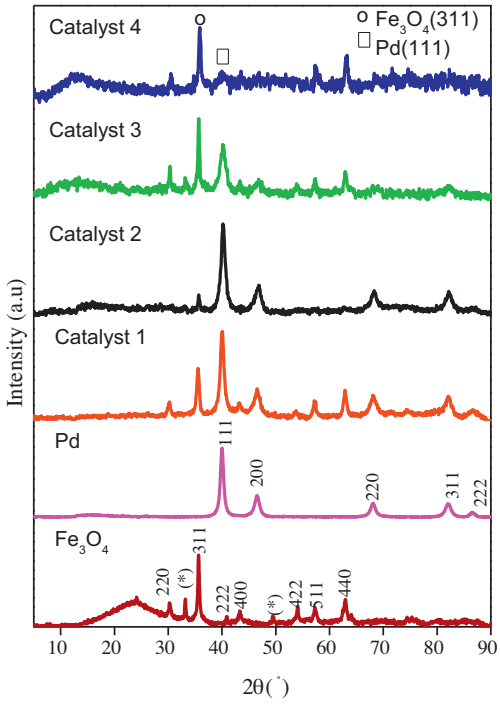

Fig. 1. XRD-patterns of the Fe_3O_4 and Pd nanoparticles and catalysts **1–4** prepared by the HH-MWI as described in the Section 2. See Table 1 for the composition of the as-prepared catalysts. The (*) in the Fe_3O_4 pattern is due to Fe_2O_3.

3.7. Procedure for the effect of catalyst concentration on the catalytic activity

Bromobenzene (50 mg, 0.32 mmol, 1 eq.) was dissolved in a mixture of 4 mL H_2O:EtOH (1:1) and placed in a 10 mL microwave tube. To this was added phenyl boronic acid (47 mg, 0.382 mmol, 1.2 eq.), and potassium carbonate (133 mg, 0.96 mmol, 3 eq.). Pd/Fe_3O_4/G nanoparticle catalysts (*X* mmol, or *Y* mol% as indicated in Fig. 5) were then added, and the tube was sealed and stirred at room temperature (r.t.). An aliquot of the reaction mixtures was taken after 30, 60, 120, 180, 240, and 300 min, diluted with 10 mL of CH_3CN and injected into the GC-MS. The percent conversions of the products were then calculated based on the consumption of bromobenzene starting materials by means of GC-MS.

4. Results and discussion

4.1.1. Characterization of the Pd/Fe_3O_4 catalysts supported on graphene

The graphene supported Pd/Fe_3O_4 catalysts prepared by the HH-MWI method were characterized using XRD, TEM and XPS analyses, and their properties were compared to the properties of the free Pd and Fe_3O_4 nanoparticles.

Fig. 1 displays the XRD patterns of the as prepared Pd and Fe_3O_4 nanoparticles, and Catalysts **1–4** containing Pd/Fe wt% values of 48.5/51.5, 18.4/22.6, 7.6/32.4, and 4.8/35, respectively (Pd content was determined by ICP-MS). The diffraction patterns of all the nanoparticles both free-standing and anchored on graphene sheets feature strong reflections indicating that all the prepared catalysts are well-crystalline. The Pd nanoparticles show the typical fcc pattern of crystalline Pd particles (JCPDS-46-1043). The Fe_3O_4 nanoparticles show the characteristic peaks for the spinal Fe_3O_4 phase (ICCD-00-003-0863) in addition to a small percentage of the α-Fe_2O_3 phase as indicated by the 2θ peaks at 33.3 and 49.6 (JCPDS-33-0664). The XRD pattern of the spinal Fe_3O_4 phase is characterized by seven peaks at 18.3°, 30.2°, 35.5°, 43.2°, 53.7°, 57.1° and 62.8°, corresponding to the (1 1 1), (2 2 0), (3 1 1), (4 0 0), (4 2 2), (5 1 1), and (4 4 0) planes [40,41].

Catalyst-**1** (Pd/Fe wt% of 48.5/51.5) which does not contain graphene, shows peaks due to Pd and Fe_3O_4 with no indication of the presence of the α-Fe_2O_3 phase. Catalyst-**2** (Pd/Fe/G wt% of 18.4/22.6/60.0) shows a decrease in the intensity of the Fe_3O_4 peaks consistent with the lower Fe content in comparison with catalyst-**1**. Catalyst-**4** shows small intensities of the Pd peaks consistent with the lowest content of Pd of 4.8 wt% as determined by the ICP-MS analysis. Catalyst-**3** shows higher intensities of the Pd peaks relative to catalyst-**4** in agreement with the higher Pd content of 7.6 wt%. Both Catalysts **3** and **4** show a small and very broad peak around $2\theta = 15°$ which suggests the presence of a minor component of partially reduced GO. GO is characterized by an XRD peak at $2\theta = 10.0°$ corresponding to a d-spacing of 8.1 Å resulting from the insertion of the hydroxyl and epoxy groups between the graphite sheets [24]. The incomplete disappearance of this peak and the shift to higher 2θ value suggest that a small amount of partially reduced GO may be present in Catalysts-**3** and **4**.

Fig. 2 displays representative TEM images of several unsupported and supported nanoparticles prepared by the MWI-assisted chemical reduction of $Pd(NO_3)_2$ or $Fe(NO_3)_3$ using hydrazine hydrate as a reducing agent. The unsupported Pd nanoparticles (Fig. 2(a)) show a significant degree of aggregation although the primary particles have small sizes in the range of 6–8 nm. In the case of Fe_3O_4, (Fig. 2(b)), most of the nanoparticles have irregular shapes with diameters between 25 and 30 nm and a few have a hexagonal plate shape. Interestingly, a 10 wt% Pd supported on Fe_3O_4 nanoparticles show small particles and improved dispersion as shown in Fig. 2(c). However, the simultaneous reduction of the metal ions and GO using HH under MWI results in well-dispersed nanoparticles supported on graphene as shown in Fig. 2(d) and Fig. 2(e) for 5 wt% Pd and 5 wt% Fe_3O_4, respectively supported on graphene. Even with higher metal/metal oxide loadings such as 10 wt% Pd and 20 wt% Fe_3O_4 nanoparticles, good dispersion of the nanoparticles on the large surface area of graphene is evident as shown in Fig. 2(f).

Fig. 3 displays TEM images of Catalysts **1–4**. From the statistical analysis of several TEM images, the mean sizes of the Pd and Fe_3O_4 nanoparticles dispersed on graphene were calculated for the four catalysts. Catalyst-**1** shows aggregated nanoparticles with a broad size distribution including 12–15 nm Pd nanoparticles and 30–45 nm Fe_3O_4 nanoparticles. For Catalyst-**2**, the particle size of Pd and Fe_3O_4 nanoparticles range from 8–12 nm and 20–25 nm, respectively as shown in Fig. 3(b). Catalyst-**3,** which contains 7.6 wt% Pd and 30 wt% Fe_3O_4, shows the smallest particle sizes (4–6 nm and 12–16 nm for the Pd and Fe_3O_4 nanoparticles, respectively) and the best dispersion among the four catalysts as shown in Fig. 3(c). Catalyst-**4**, which contains 4.8 wt% Pd and 34 wt% Fe_3O_4 has 8–12 nm Pd nanoparticles and 18–22 nm magnetite nanoparticles as shown in Fig. 3(d). It is clear that the presence of graphene has a tremendous effect in forming smaller Pd and Fe_3O_4, and in maintaining good dispersion of the particles on the graphene surface. It is also clear that the particle size and the degree of agglomeration are very sensitive to the concentrations of Pd and Fe_3O_4 nanoparticles supported on graphene. Both catalysts **3** and **4** show good dispersion of the nanoparticles on the graphene surface but Catalyst **3** shows the smallest particle sizes probably because of the decreased amount of Fe_3O_4 relative to catalyst **4**. It should be noted that one of the important features of our catalyst preparation is the production of large graphene sheets (several microns) homogenously decorated with well-dispersed Pd and Fe_3O_4 nanoparticles as shown in the TEM images of Figs. 3(b–d).

To characterize the surface composition of the supported nanocatalysts, we carried out XPS measurements as shown in Fig. 4.

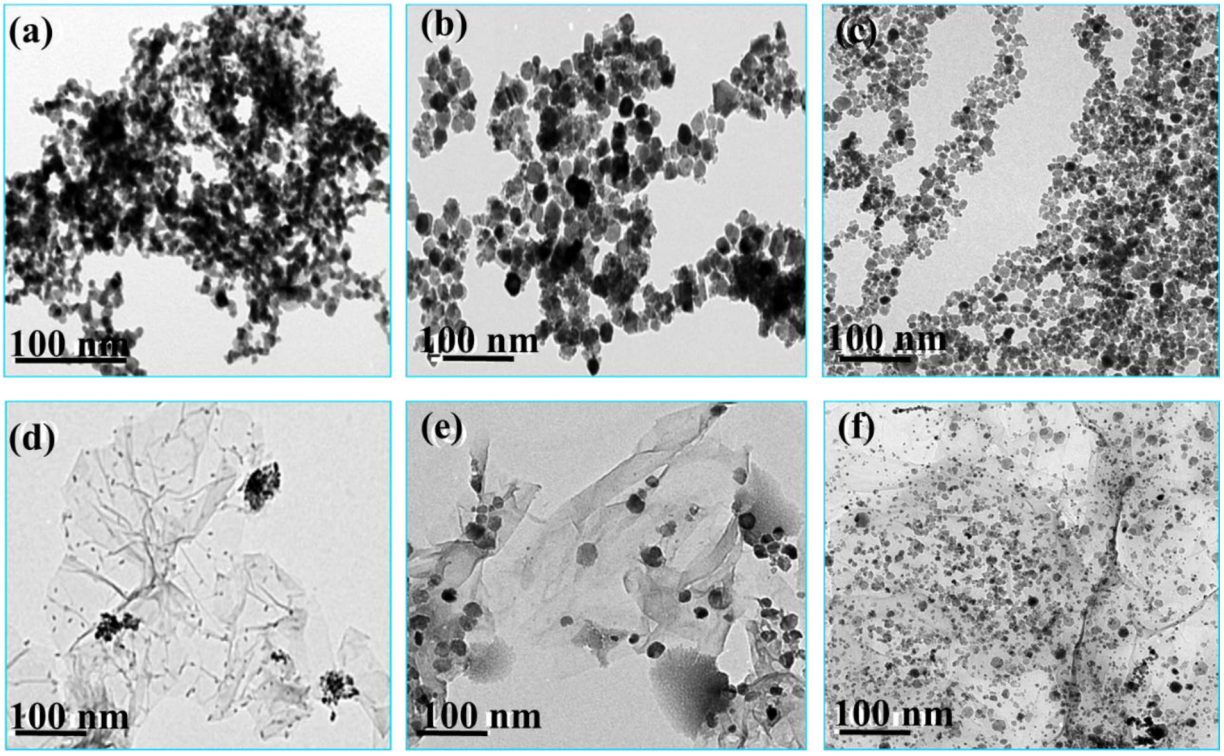

Fig. 2. TEM–images of (a) Pd, (b) Fe_3O_4, (c) 10% Pd in Fe_3O_4, (d) 5% Pd/G, (e) 5% Fe_3O_4/G, and (f) 10% Pd and 20% Fe_3O_4/G.

Fig. 4a compares the C 1s XPS spectra of GO and catalysts **2**, **3** and **4** supported on reduced GO. The compositional analysis of the C 1s spectra of the four samples is also shown in Fig. 4a. The GO spectrum shows peaks corresponding to oxygen containing groups between 285.5 and 289 eV, in addition to the sp^2-bonded carbon C=C at 284.5 eV. Typically, peaks at 285.6, 286.7, 287.7 and 289 are assigned to the C1s of the C—OH, C—O, C=O, and HO–C=O groups, respectively [42–44]. As shown from the compositional

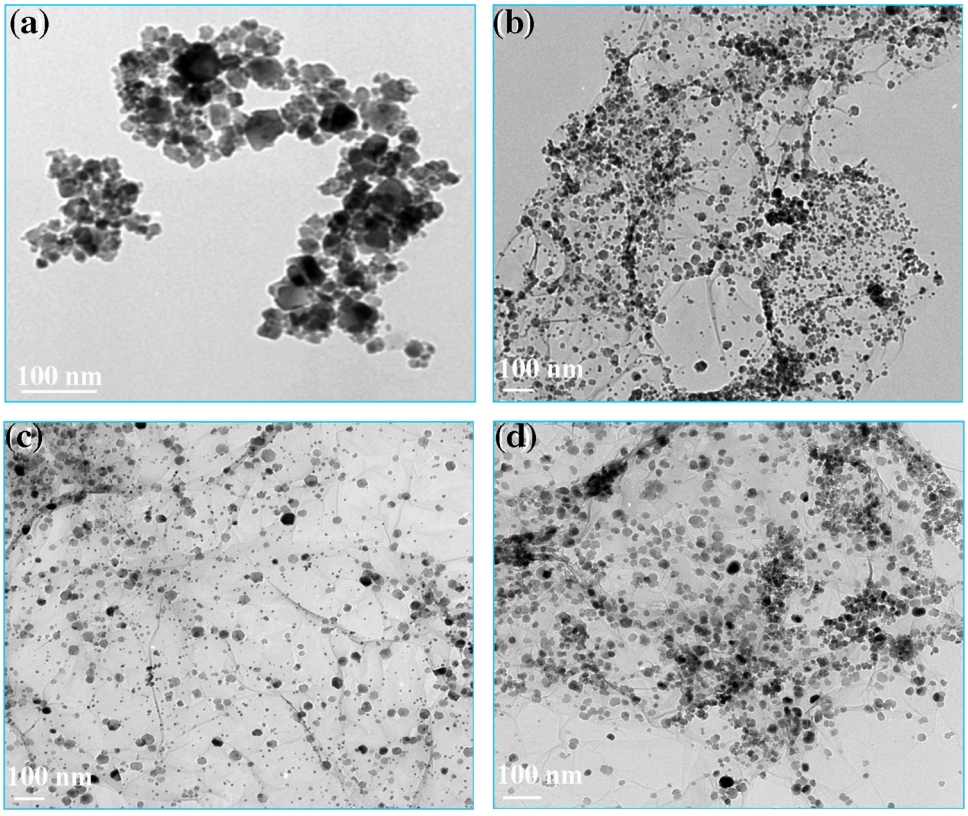

Fig. 3. TEM–images of: (a) Catalyst **1**, (b) Catalyst **2**, (c) Catalyst **3**, and (d) Catalyst **4**. See Table 1 for the composition of the as-prepared catalysts.

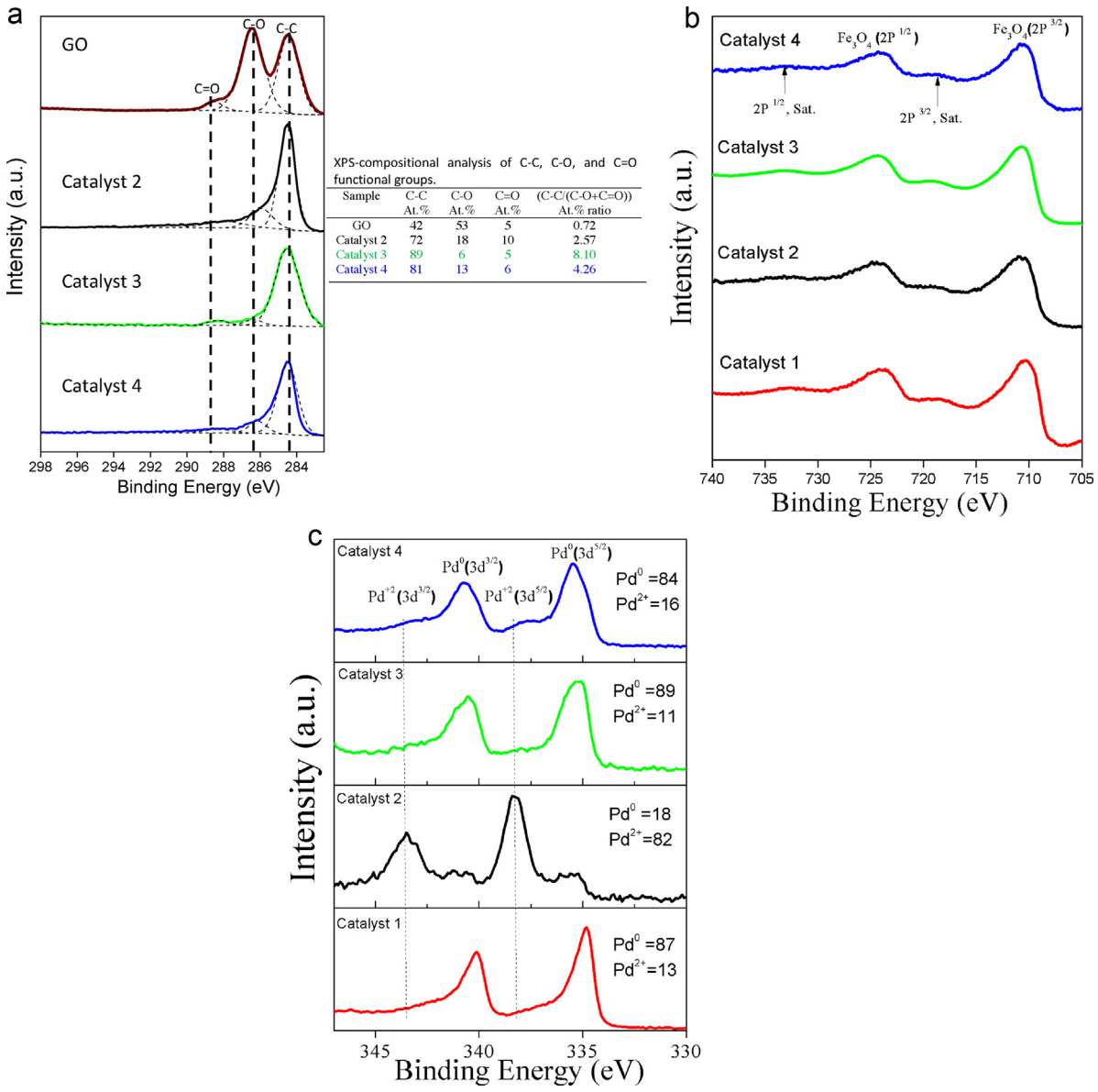

XPS-compositional analysis of C-C, C-O, and C=O functional groups.

Sample	C-C At.%	C-O At.%	C=O At.%	(C-C/(C-O+C=O)) At.% ratio
GO	42	53	5	0.72
Catalyst 2	72	18	10	2.57
Catalyst 3	89	6	5	8.10
Catalyst 4	81	13	6	4.26

Fig. 4. a. Comparison of the XPS (C1s) binding energies of GO and those of catalysts **2–4**. See Table 1 for the composition of the as-prepared catalysts.
Fig. 4b. Comparison of the XPS (Fe-2p) binding energies of catalysts **1–4**. See Table 1 for the composition of the as-prepared catalysts.
Fig. 4c. Comparison of the XPS (Pd-3d) binding energies of catalysts **1–4**. See Table 1 for the composition of the as-prepared catalysts. The Pd^0 and Pd^{2+} values shown above are in atomic % as calculated from the XPS peak analysis for each catalyst.

analysis, the at% of the C—C to the (C—O + C=O) intensity ratio in the GO sample used in the preparation of catalysts **2**, **3** and **4** is 0.72. This ratio increases to 2.57, 8.1 and 4.26 in catalysts **2**, **3** and **4,** respectively indicating that most of the oxygen-containing groups in GO are removed in catalyst **3** following the MW-assisted reduction by HH. However, the small (C—C)/(C—O + C=O) intensity ratio obtained in catalyst **2** suggests that a significant amount of the oxygen-containing groups in GO are still present and therefore, catalyst **2** appears to be supported on partially reduced GO.

Fig. 4b shows the Fe 2p XPS spectra of the four catalysts. The data reveals the presence of Fe(III) as indicated by the observed peaks at 724.2 eV and 710.5 eV corresponding to the binding energies of the $2p^{1/2}$ and $2p^{3/2}$ electrons, respectively along with small satellite peaks around 732.5 eV and 718.5 eV associated with the $2p^{1/2}$ and $2p^{3/2}$ electron binding energies. The broad Fe(III) $2p^{3/2}$ peak centered at 710.5 eV probably contains a contribution from the Fe(II) $2p^{3/2}$ which normally occurs at ~708 eV. The absence of significant peaks in the 718–720 eV range, characteristic of γ-Fe_2O_3, confirms the formation of the crystalline Fe_3O_4 phase in the four catalysts, consistent with the values reported in the literature [45].

Fig. 4c displays the XPS spectra of the Pd-3d electron in the four catalysts listed in Table 1. For catalyst **1**, the observed binding energies of 334.8 eV and 340.1 eV indicate the presence of 82% Pd^0 and 18% Pd^{2+}. However, the observed binding energies are slightly lower than the binding energies of Pd 3d electrons in pure Pd nanoparticles where the values of 335 eV and 341.1 eV have been reported for Pd^0 and Pd^{2+}, respectively [46]. The decrease in the binding energy of the Pd 3d electron in the Pd/Fe_3O_4 catalyst indicates that the Pd in the supported catalyst is more electron rich than in pure Pd nanoparticles [46]. This could be due to electron transfer from Fe_2O_3 to Pd consistent with similar results obtained for the Pd/Fe_2O_3 hybrid nanocatalysts prepared by a seed-mediated process [46], and also for Pd nanoparticles grown by vapor phase deposition on ordered crystalline Fe_3O_4 films [47]. The high Pd(0)/Pd(II) ratio in catalyst **1** in spite of the high content of

Pd (48.5 wt%) suggests that the reduction of Pd(II) is assisted by the formation of Fe_3O_4.

Catalyst **2** has the highest amount of Pd(II) (82%) as a result of the inefficient reduction of the Pd ions in the presence of GO due to the use of an insufficient amount of hydrazine hydrate. This catalyst also shows a partial reduction of the GO support, as shown in Fig. 4a, because of the competition between the large amount of the Pd ions and GO for the small amount of the reducing agent. This behavior is consistent with previous results which indicate that the reduction of Pd^{2+} ions is inefficient in the presence of partially reduced GO [18]. This is also consistent with the XPS data of catalyst **3** which shows the highest Pd(0)/Pd(II) ratio of 8.1 and also the highest C/O ratio of 8.1 in the reduced GO. Although catalyst **4** contains the smallest Pd loading (4.8 wt%), it has a smaller Pd(0)/Pd(II) ratio (5.3) than in catalyst **3** (8.1). The relatively smaller Pd(0)/Pd(II) ratio in catalyst **4** appears to be related to the smaller C/O ratio (4.3) of the reduced GO in catalyst **4** as compared to same ratio in catalyst **3** (8.1).

Table 2 summarizes the XRD, TEM and XPS characterization data for the catalysts **1–4**. It is clear from the results that catalyst **3,** which contains 7.6 wt% Pd, possesses the smallest Pd and Fe_3O_4 particles' sizes, the largest Pd(0)/Pd(II) ratio, the largest C/O ratio of the reduced GO support, and the best homogeneous distribution of Pd nanoparticles and dispersion on the surface of the support. These results suggest that catalyst **3** should exhibit the highest catalytic activity among the four catalysts as will be confirmed in Section 4.1.2.

4.1.2. Effect of the catalyst concentrations on the Suzuki cross coupling reactions

The catalytic activity of the four $Pd/Fe_3O_4/G$ catalysts were investigated using the Suzuki cross coupling reaction of bromobenzene and phenylboronic acid (Eq. (1)) in a mixture of H_2O:EtOH (1:1) at room temperature using various catalyst concentrations and the results are displayed in Fig. 5.

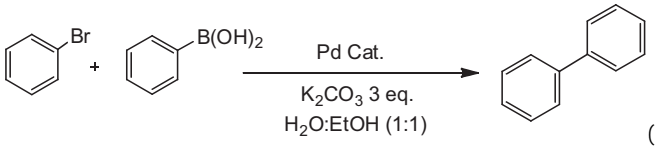

(1)

With 0.3 mol% catalyst loading, catalyst **3** demonstrates 100% conversion to the biphenyl product within 45 min reaction time at room temperature. Under the same conditions, catalyst **4** shows 96% conversion after 90 min at room temperature. On the other hand, catalysts **2** and **1** display only 95% and 60% conversion, respectively, after 5 h reaction time at room temperature.

The effect of the graphene support is clearly evident by comparing the performance of catalyst 1 which includes the highest Pd wt% (48.5%) but no GO or RGO and catalysts **2–4** which include less Pd contents but are supported on partially reduced GO (catalyst **2**) or RGO (catalysts **3** and **4**). The higher activity of catalysts **3** and **4** over catalyst **2** is most likely due to the high Pd(II)/Pd(0) ratio and the partial reduction of GO in catalyst **2**. The correlation of the high activity with the concentration of Pd(0) in the catalyst can be also demonstrated by comparing the activity of catalyst **3** (Pd(0)/Pd(II) = 8.1) and catalyst **4** (Pd(0)/Pd(II) = 5.3). Of course, the high activity of catalyst **3** is also related to having the smallest Pd nanoparticles' size (4–6 nm) and the best dispersion on the surface of the RGO.

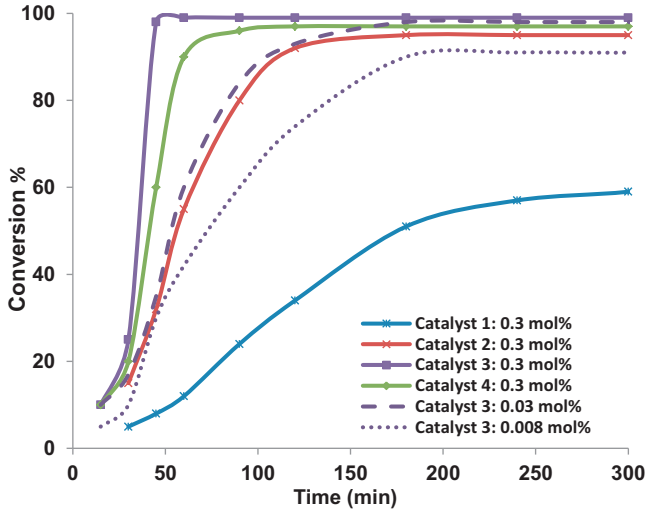

Fig. 5. % Conversion of the reactants to the biphenyl product in the Suzuki Coupling (Eq. (1)) for catalysts **1–4** and for different concentrations of catalyst **3**. See Table 2 for the properties of catalysts **1–4**.

At lower catalyst concentrations of 0.03 mol%, catalyst **3** was capable of affording a 93% conversion after 2 h reaction time at room temperature. Further decrease of the concentration of catalyst **3** to 0.008 mol% provided a 91% conversion to the biphenyl product after 5 h reaction time at room temperature. At this low catalyst loading (0.008 mol%), catalyst **3** yielded 74% and 100% conversion to the product at 80 °C after 5 min and 10 min, respectively of reaction time under microwave heating. These results demonstrate an excellent catalytic activity of catalyst 3 with a turn over number (TON) of 9250 and a turn over frequency (TOF) of 111,000 h^{-1}.

To investigate the extent of Pd leaching from catalyst 3, Eq. (1) was carried out in the presence of 0.3 mol% catalyst at 80 °C for 10 min under microwave heating. Upon the completion of the reaction period, the mixture was hot filtered over the celite and the Pd content was determined in the filtrate to be 150 ppm based on the ICP-MS analysis. Moreover, the filtrate solution was subjected to the same reaction using fresh reagents of bromobenzene and phenylboronic acid, and no further catalytic activity was observed in this solution after heating the fresh reaction mixture to 80 °C for 10 min under microwave irradiation. This confirms the lack of

Table 2
Properties of Catalysts **1–4** used for the Suzuki Cross-Coupling Reactions.

Catalyst #	Pd (wt%)[a] Particle size	Fe_3O_4 (wt%) Particle size	XRD Ratio Pd(1 1 1)/Fe_3O_4(3 1 1)	XPS Ratio Pd(0)/Pd(II)	XPS Ratio C/O
Catalyst **1**	(48.5) 12–15 nm	(51.5) 30–45 nm	1.50	6.70	
Catalyst **2**	(18.4) 8–12 nm	(20) 20-35 nm	5.60	0.22	2.6
Catalyst **3**	(7.6) 4-6 nm	(30) 12-16	0.75	8.10	8.1
Catalyst **4**	(4.8) 8-12 nm	(34) 18-22 nm	0.15	5.25	4.3

[a] As determined by ICP-MS.

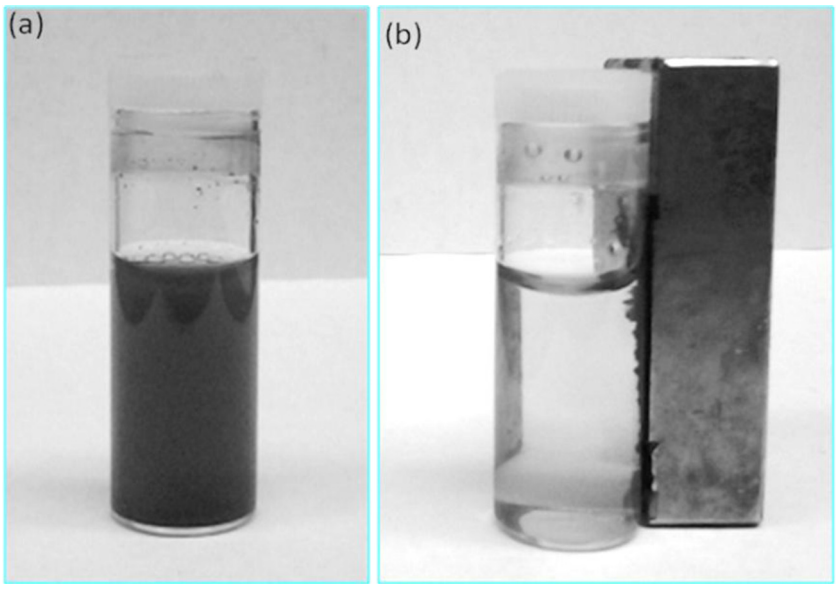

Fig. 6. (a) The reaction mixture using 0.3 mol% of catalyst 3 after the completion of Eq. (1). (b) Separation of spent catalyst from reaction mixture using a simple magnet.

residual activity in the reaction mixture after the catalyst removal which is consistent with the very small amount of Pd content in solution determined by ICP-MS.

The above results clearly demonstrate the superior catalytic properties of the Pd/Fe_3O_4/graphene system (catalyst **3**) as a truly heterogeneous catalyst for the for Suzuki cross-coupling reactions. The catalyst contains 7.6 wt% Pd nanoparticles with 4–6 nm diameters and mostly Pd(0) oxidation state supported on both Fe_3O_4 nanoparticles with 12–16 nm diameters and highly reduced GO containing C/O ratio of 8.1. These combined properties produce active Pd nanoparticles well-dispersed on the large specific surface area of the reduced graphene oxide. The 7.6 wt% Pd/Fe_3O_4/G catalyst exhibits a very high TOF of 111,000 h^{-1} at 80 °C comparable to that of the 7.9 wt% Pd/G catalyst previously prepared using the same MW-assisted chemical reduction method which resulted in a TOF of 108,000 h^{-1} at 80 °C [18]. However, the added advantage of the current Pd/Fe_3O_4/G catalysts are the ability to magnetically separate the catalyst from the reaction mixture and recycle the catalyst multiple times without loss of catalytic activity as will be demonstrated in Section 4.2.

Table 3
Recycling experiments for the Suzuki Coupling Eq. (1) using 0.5 mol% of Catalysts **3** and **4.**

Run	Conversion (%)[b] **Catalyst 3**	Conversion (%)[b] **Catalyst 4**
1	100	100
2	100	96
3	93	94
4	93	93
5	92	92
6	92	82
7	92	79
8	89	–
9	81	–
10	80	–

[a]Bromobenzene (50 mg, 0.32 mmol), boronic acid (47 mg, 0.382 mmol, 1.2 eq.), potassium carbonate (133 mg, 0.96 mmol, 3 eq.), and Pd/Fe_3O_4/G (2.17 mg, 1.16 μmol, 0.5 mol%) in 4 mL (H_2O:EtOH) (1:1) were heated at 80 ° C (MWI) for 10 min.

[b] Conversion was determined by GC–MS.

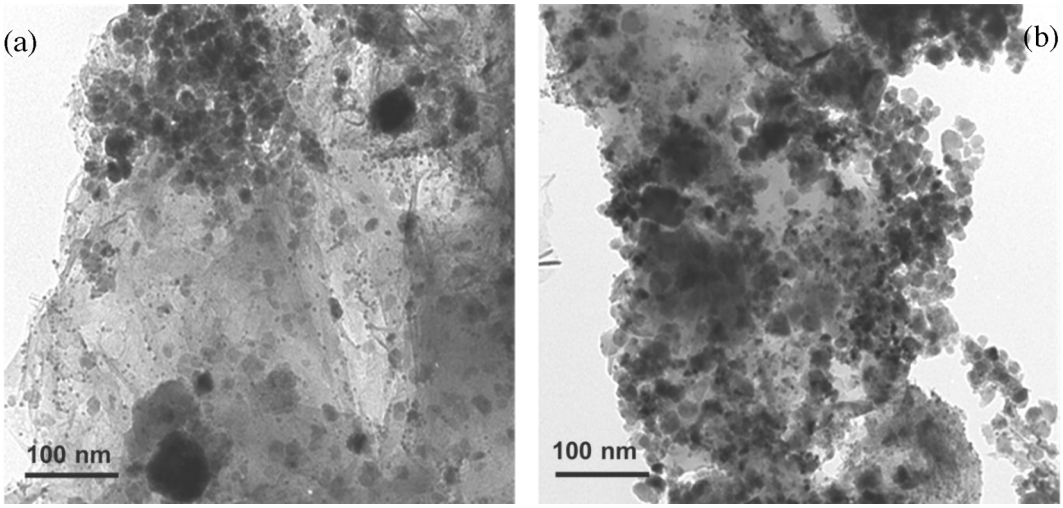

Fig. 7. TEM images of the spent Pd/Fe_3O_4/G catalysts: (a) catalyst **3** after the tenth run and (b) catalyst **4** after the seventh run.

Table 4
Diversity of the Suzuki coupling reactions using catalyst **3**.[a]

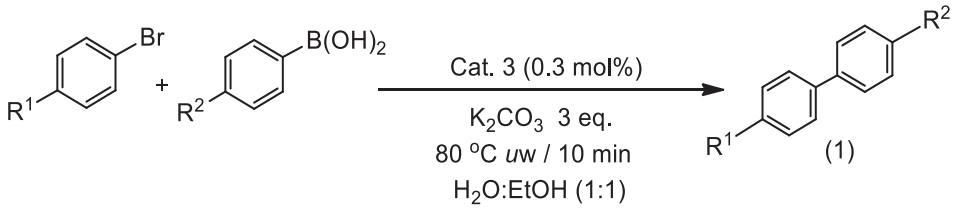

cpd	Aryl-halide	Boronic acid	Eq. (1) (%)[c]
a[b]	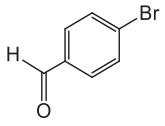	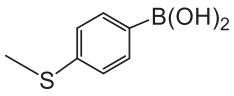	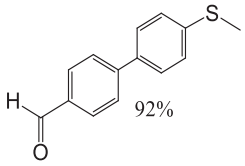 92%
b[b]	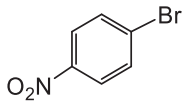	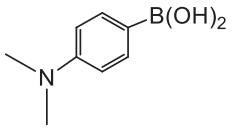	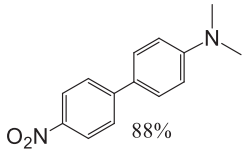 88%
c	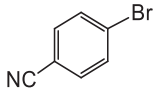	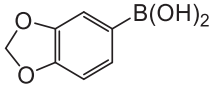	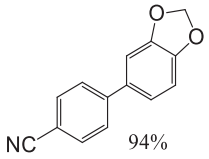 94%
d	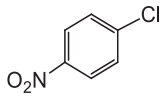	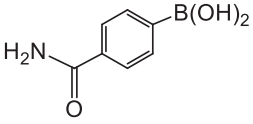	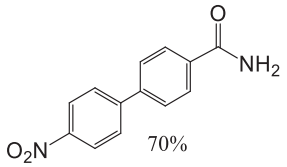 70%
e	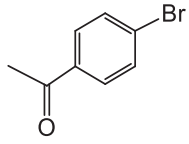	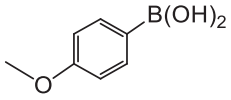	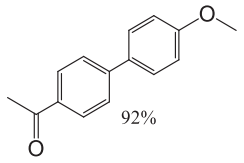 92%
f	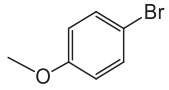	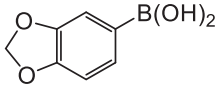	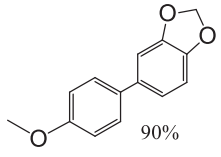 90%

[a] Aryl halide (0.32 mmol), Boronic acid (0.382 mmol), potassium carbonate (0.96 mmol), and $Pd/Fe_3O_4/G$ (0.3 mol%) in 4 mL (H_2O:EtOH) (1:1) was heated at 80 °C under microwave for 10 min.
[b] Reactions were completed at r.t. after 30 min.
[c] Isolated yields.

4.2. Magnetic separation & recyclability of the Pd/Fe_3O_4/graphene catalysts

One of the major advantages for using heterogeneous catalysis is the ability to remove the catalyst from the reaction mixture and reuse it in subsequent runs. However, the isolation of the heterogeneous catalysts from the reaction mixture by conventional filtration methods is inefficient and time consuming. The current Pd/Fe_3O_4 nanoparticles supported on graphene could provide an efficient and fast procedure to magnetically separate the catalysts from the reaction mixture. To characterize the magnetic properties of the $Pd/Fe_3O_4/G$ catalysts, we measured the magnetization curves of the as-prepared Fe_3O_4 free nanoparticles and the 7.6 wt% $Pd/Fe_3O_4/G$ (catalyst **3**) at room temperature using the vibrating sample magnetometer (VSM) analysis (Supporting Information). The measured saturation magnetization as a function of the external magnetic field shows that the 7.6 wt% Pd/30 wt% Fe_3O_4/G catalyst has saturation magnetization (Ms) of 12.0 emu/g which is about 25% of the Ms value of the Fe_3O_4 nanoparticles at room temperature as shown in Fig. S1 (Supporting Information). The measured Ms value of catalyst **3** is comparable to the reported saturation magnetization for spherical magnetite nanoparticles supported on graphene (10.2 emu/g) [48]. For the present application of the magnetic separation of the $Pd/Fe_3O_4/G$ catalyst, the measured magnetization is

Table 5
Diversity of the Heck coupling reactions using catalyst **3**.[a]

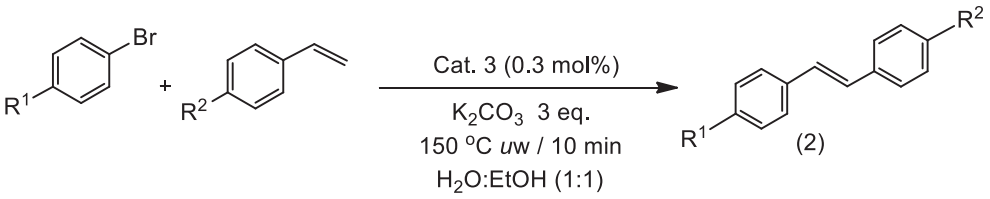

cpd	Aryl-halide	Alkene	Eq. (2) (%)[b]
a	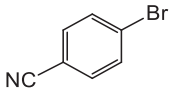	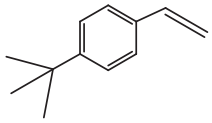	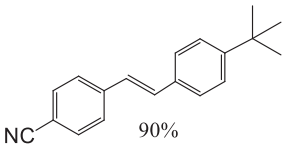 90%
b	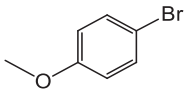	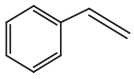	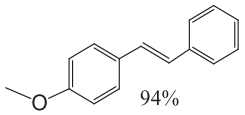 94%
c	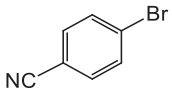	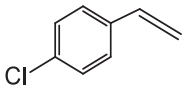	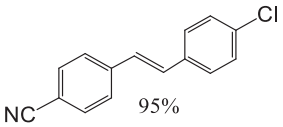 95%
d	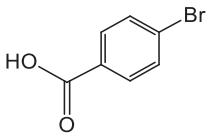	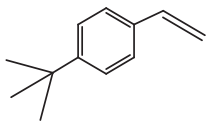	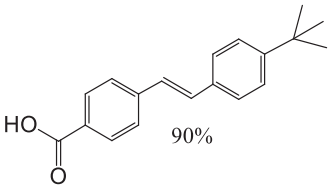 90%
e	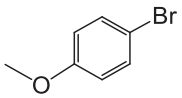	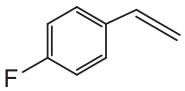	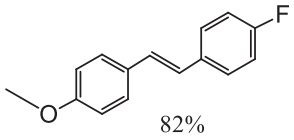 82%
f	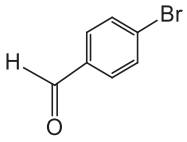	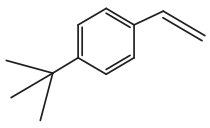	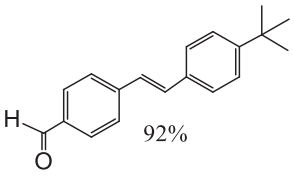 92%

[a] Aryl bromide (0.32 mmol), alkene (0.64 mmol), potassium carbonate (0.96 mmol), Pd/Fe_3O_4/G (0.3 mol%) in 4 mL (H_2O:EtOH) (1:1) was heated under microwave at 150 °C for 10 min.
[b] Isolated yields.

sufficient for the removal of the catalyst from the reaction mixture using a simple laboratory magnet as shown in Fig. 6. It is clear that all the catalyst particles can be collected from the reaction mixture using an external magnet as shown in Fig. 6-b.

The recyclability of the Pd/Fe_3O_4/G catalysts was examined for Eq. (1) using 0.5 mol% of catalysts **3** and **4** at 80 °C for 10 min. After the reaction, the catalyst was easily removed from the reaction mixture using a simple magnet as shown in Fig. 6, washed further with EtOH to remove the product from the surface of the nanoparticles, and reused in the next reaction run. The sequence of preparing the reaction mixture, carrying out the reaction using the MW reactor, the magnetic separation of the spent catalyst, and the isolation of the catalyst is shown in Fig. S2 (Supporting Information).

The results of the recyclability experiments for catalysts **3** and **4** are shown in Table 3. While both catalysts demonstrated a significant number of recycles with high activity, catalyst **3** showed a greater recyclability of up to eight subsequent reaction runs, achieving nearly 90% or higher yield of the product as shown in Table 3. The catalytic activity of catalyst **3** was then slightly dropped to 80% conversion in the ninth and tenth runs (Table 3).

To investigate the possible deactivation mechanism of the Pd/Fe_3O_4/G catalysts following the recycling experiments, TEM images of the spent catalysts **3** and **4** after the tenth and the seventh runs, respectively were obtained as shown in Fig. 7. Both images display a significant agglomeration and accumulation of the Pd and Fe_3O_4 nanoparticles on the surface of graphene. The aggregation of the Pd nanoparticles results in diminishing the available active sites which ultimately diminishes the catalytic activity of the catalyst. In comparing the agglomeration effects of catalysts **3** and **4** after recycling, it appears that catalyst **4** shows a significant removal of the Pd and Fe_3O_4 nanoparticles from the surface of graphene indicating that the catalyst–support interaction may be weaker in catalyst **4** than in catalyst **3**. The catalyst–support interaction in these graphene-supported

catalysts is mainly determined during the MW synthesis of the catalysts which involves the simultaneous nucleation of the Pd and Fe_3O_4 nanoparticles and reduction of GO. The non-equilibrium dielectric heating during the MW-assisted chemical reduction of GO leads to structural defects in the reduced GO sheets. These defect sites, consisting of large vacancies and missing atoms, act as nucleation centers for the Pd-Fe_3O_4 composite nanoparticles which can be anchored to the graphene sheets thus decreasing their mobility under typical reaction conditions and minimizing the potential of their agglomeration and the subsequent decrease in the catalytic activity. It appears that catalyst **3** with the most reduced GO, as evident by the largest C/O ratio, may include more defect sites than catalyst **4** and this may explain the better anchoring of the Pd and Fe_3O_4 nanoparticles to the graphene surface in catalyst **3**.

4.3. Catalytic activity of the Pd/Fe_3O_4/graphene catalyst for Suzuki cross coupling reactions with functionalized reactants

The catalytic activity of the 7.6 wt% Pd/Fe_3O_4/G catalyst was further examined for other Suzuki cross coupling reactions employing a diverse range of functionalized aryl halide and aryl boronic acid substrates. As shown in Table 4, the reactions of aryl bromide with aryl boronic acid were carried out in the presence of 0.3 mol% of catalyst **3** using potassium carbonate (3 eq.) as the base in H_2O:EtOH (1:1), an environmentally benign solvent system. All reactions were resulted in the formation of the corresponding biphenyl products in a high yield. Diversity of the functional groups on the phenyl ring can be modified from both aryl bromide and phenyl boronic acid substrates. For instance, using aryl halides containing aldehyde (**1a**), ketone (**1e**), nitro (**1b**), and nitrile (**1c**) substituents afforded the corresponding Suzuki products in high yields. Notably the reactions with electron withdrawing substituents such as aldehyde (**1a**) and nitro (**1b**) groups can be performed at room temperature within 30 min. It should be noted that the chloro- substituted aryl halide can also undergo Suzuki reaction in a relatively good yield (**1d**). In addition, the aryl boronic acid bearing different functionality such as dimethyl amino (**1b**), thiomethyl (**1a**), 4-amino carbonyl (**1d**), and *p*-methoxy (**1e**) can be effectively applied in these coupling reactions. The remarkable reactivity of 7.6 wt% Pd/Fe_3O_4/G nanoparticles in Suzuki cross coupling reactions with various functionalized substrates also proved to exhibit a significant impact on the turn over number (TON) and turn over frequency (TOF) for these reactions. As such, performing the reaction of (**1a)** at lowest catalyst loading of 0.008 mol% at 80 °C for 5 min under microwave irradiation afforded 65% conversion to the product using H_2O:EtOH as the solvent system. These results led to a turn over number (TON) of 8100 and a turn over frequency (TOF) of 97,500 h^{-1} for the formation of (**1a**). Likewise, the TON and TOF numbers were also examined for other electron withdrawing (**1b**) and electron rich (**1f**) aryl halides under the similar reaction conditions using 0.008 mol% of the catalyst. These reactions also afforded conversions of 70% and 78% at 80 °C microwave irradiation for 5 min for **1b** and **1f**, respectively, which resulted in high TON/TOF numbers of 8750/105,000 h^{-1} for **1b** and 9750/117,000 h^{-1} for **1f**. The high TON/TOF numbers obtained in these reactions provide strong evidence for the superior catalytic activity of the 7.6 wt% Pd/Fe_3O_4/G catalyst in Suzuki cross coupling reactions involving different functionalized substrates under microwave heating at low catalyst concentration and in a short reaction time.

4.4. Catalytic activity of the Pd/Fe3O4/graphene catalyst for Heck coupling reactions

The utility of the 7.6 wt% Pd/Fe_3O_4/G catalyst was further evaluated for the Heck coupling reactions. While Heck reactions are typically performed in the presence of homogeneous palladium catalyst using appropriate ligands, the use of the Pd/Fe_3O_4/G catalyst under ligand-free microwave irradiation conditions could provide an efficient and facile approach for the synthesis of key pharmaceutical compounds. As illustrated in Table 5, the Heck reactions of aryl bromides with diverse range of substituted olefin were studied using 0.3 mol% of catalyst **3**, and potassium carbonate (3 eq.) in a mixture of H_2O:EtOH (1:1) at 150 °C for 10 min under microwave heating. Both electron-rich (**2b**) and electron-poor (**2a, 2d, 2f**) aryl bromide substrates can easily undergo the Heck reactions with substituted alkenes affording the coupling products in excellent yields.

The above results clearly demonstrate the high activity and excellent recyclability of the Pd/Fe_3O_4/graphene catalysts as truly heterogeneous catalysts for the Suzuki and Heck coupling reactions. The origin of the enhancement in activity and stability of these graphene-supported catalysts is not fully understood. Traditional surface area and dispersion factors may not account for this activity, and the emergence of electronic factors that fundamentally alter interactions with the support need to be investigated. We postulate that the defect sites on the surface of graphene provide an excellent environment for the nucleation of surface active metal nanoparticles and as a result, play a major role in imparting exceptional catalytic properties and stability to the metal–graphene catalysts. It is now well established that the chemical reduction of GO results in the formation of graphene nanosheets with a significant number of defect sites including vacancies, disorder, defective edges, and others [27–29]. The use of MWI in our synthesis of the graphene-supported catalysts is expected to enhance the formation of graphene defects especially in the presence of metal nanoparticles due to the non-equilibrium heating and the formation of energetic hot spots [35–38].

5. Conclusions

In summary, we have developed an efficient method to generate highly active Pd/Fe_3O_4 composite nanoparticles supported on graphene (Pd/Fe_3O_4/G) by microwave assisted chemical reduction of the corresponding aqueous mixture of palladium nitrate, ferric nitrate and dispersed graphene oxide nanosheets. We have shown that the palladium/ferric nitrate concentration ratio used in the graphene oxide solution has intrinsic effects on the particle size, distribution, the degree of reduction of both the Pd ions and GO, and subsequently on the catalytic activity of supported catalysts. The Pd/Fe_3O_4/G catalyst containing 7.6 wt% Pd exhibits excellent catalytic activity toward the Suzuki cross coupling reaction with a high turnover number (TON) of 9250 and turnover frequency (TOF) of 111,000 h^{-1}. This catalyst offers a number of advantages including high reactivity, recyclability of up to ten times, mild reaction conditions, and short reaction times in an environmentally benign solvent system. Furthermore, the magnetic properties imparted by the Fe_3O_4 component of the catalyst enables the catalyst to be easily isolated and recycled, thus greatly simplifying the ability to purify the reaction products and increasing the economic value of the catalyst. This catalyst also provided excellent yields over a broad range of highly functionalized substrates in both Suzuki and Heck coupling reactions.

Supplementary material

Magnetic properties of the 7.6 wt% Pd/Fe_3O_4/G catalyst (Fig. S1), photographs showing the sequence of magnetic separation of the catalyst from the reaction mixture (Fig. S2), and NMR data for identification of the reaction products.

Acknowledgements

We thank the National Science Foundation (OISE-1002970) for the support of this work. We gratefully acknowledge Dr. Joseph Terner (VCU) for his kind help in the ICP-MS measurements.

Appendix A. Supplementary data

Supplementary data associated with this article can be found, in the online version, at http://dx.doi.org/10.1016/j.apcata.2014.11.033.

References

[1] A. Molnar, Chem. Rev. 111 (2011) 2251–2320.
[2] A. Balanta, C. Godard, C. Claver, Chem. Soc. Rev. 40 (2011) 4973–4985.
[3] L. Yin, J. Liebscher, Chem. Rev. 107 (2007) 133–173.
[4] Special Issue on Cross Coupling: Ed: S. L. Buchwald, Acc. Chem. Res. 2008, 41, 1439-1564.
[5] K.C. Nicolaou, P.G. Bulger, D. Sarlah, Angew. Chem. Int. Ed. 44 (2005) 4442–4489.
[6] C. Garrett, K. Prasad, Adv. Synth. Catal. 346 (2004) 889–900.
[7] D.J. Cole-Hamilton, Science 299 (2003) 1702–1706.
[8] J.A. Widegren, J. Mol. Catal. A 198 (2003) 317–341.
[9] C.J. Welch, J. Albaneze-Walker, W.R. Leonard, M. Biba, J. DaSilva, D. Henderson, B.B. Laing, D.J. Mathre, S. Spencer, X. Bu, T. Wang, Org. Process Res. Dev. 9 (2005) 198–205.
[10] K. Köhler, R.G. Heidenreich, S.S. Soomro, S.S. Pröckl, Adv. Synth. Catal. 350 (2008) 2930–2936.
[11] R. Narayanan, M.A. El-Sayed, J. Phys. Chem. B. 108 (2004) 8572–8580.
[12] R. Narayanan, M. Tabor, M. El-Sayed, Top. Catal. 48 (2008) 60–74.
[13] P.J. Ellis, I.J.S. Fairlamb, S.F.J. Hackett, K. Wilson, A.F. Lee, Angew. Chem. Int. Ed. 49 (2010) 1820–1824.
[14] S. Ogasawara, S. Kato, J. Am. Chem. Soc. 132 (2010) 4608–4613.
[15] B. Cornelio, G.A. Rance, M. Laronze-Cochard, A. Fontana, J. Sapi, A.N. Khlobystov, J. Mater. Chem. A 1 (2013) 8737–8744.
[16] A.R. Siamaki, Y. Lin, K. Woodberry, J.W. Connell, B.F. Gupton, J. Mater. Chem. A 1 (2013) 12909–12918.
[17] G.M. Scheuermann, L. Rumi, P. Steurer, W. Bannwarth, R. Mülhaupt, J. Am. Chem. Soc. 131 (2009) 8262–8270.
[18] A.R. Siamaki, A.E.R.S. Khder, V. Abdelsayed, M.S. El-Shall, B.F. Gupton, J. Catal. 279 (2011) 1–11.
[19] S. Moussa, A.R. Siamaki, B.F. Gupton, M.S. El-Shall, ACS Catal. 2 (2012) 145–154.
[20] M.S. El-Shall, Heterogeneous catalysis by metal nanoparticles supported on graphene, Chapter 10, in: C.N.R. Rao, A.K. Sood (Eds.), Graphene: Synthesis, Properties and Applications, Wiley-VCH, 2013, pp. 303–338.
[21] A. Schaetz, M. Zeltner, W.J. Stark, ACS Catal. 2 (2012) 1267–1284.
[22] D.S. Su, S. Perathoner, G. Centi, Chem. Rev. 113 (2013) 5782–5816.
[23] P.V. Kamat, J. Phys. Chem. Lett. 1 (2010) 520–527.
[24] H.M.A. Hassan, V. Abdelsayed, A.E.R. Khder, K.M. AbouZeid, J. Terner, M.S. El-Shall, S.I. Al-Resayes, A.A. El-Azhary, J. Mater. Chem. 19 (2009) 3832–3837.
[25] S. Moussa, V. Abdelsayed, M.S. El-Shall, Chem. Phys. Lett. 510 (2011) 179–184.
[26] S.O. Moussa, L.S. Panchakarla, M.Q. Ho, M.S. El-Shall, ACS Catal. 4 (2014) 535–545.
[27] A. Bagri, C. Mattevi, M. Acik, Y.J. Chabal, M. Chhowalla, V.B. Shenoy, Nat. Chem. 2 (2010) 581–587.
[28] F. Banhart, J. Kotakoski, A.V. Krashennnikov, ACS Nano 5 (2011) 26–41.
[29] G. Kim, S.-H. Jhi, ACS Nano 5 (2011) 805–810.
[30] M.B. Gawande, P.S. Brancoa, R.S. Varma, Chem. Soc. Rev. 42 (2013) 3371–3393.
[31] S. Chen, R. Si, E. Taylor, J. Janzen, J. Chenm, J. Phys. Chem. A 116 (2012) 12969–12976.
[32] J. Dong, Z.H. Xu, S.M. Kuznicki, Adv. Funct. Mater. 19 (2009) 1268–1275.
[33] X. Li, X. Wang, S. Song, D. Liu, H. Zhang, Chem. Eur. J. 12 (2012) 7601–7607.
[34] J. Hu, Y. Wang, M. Han, Y. Zhou, X. Jiang, P. Sun, Catal. Sci. Technol. 2 (2012) 2332–2340.
[35] Y.-J. Zhu, F. Chen, Chem. Rev. 114 (2014) 6462–6555.
[36] V. Abdelsayed, A. Aljarash, M.S. El-Shall, Chem. Mater. 21 (2009) 2825–2834.
[37] N.P. Herring, K. AbouZeid, M.B. Mohamed, J. Pinsk, M.S. El-Shall, Lagmuir 27 (2011) 15146–15154.
[38] Y. Tsukahara, A. Higashi, T. Yamauchi, T. Nakamura, M. Yasuda, A. Baba, Y. Wada, J. Phys. Chem. C. 114 (2010) 8965–8970.
[39] W.S. Hummers Jr., R.E. Offerman, J. Am. Chem. Soc. 80 (1958) 1339–1340.
[40] S. Sun, H. Zeng, J. Am. Chem. Soc. 124 (2002) 8204–8205.
[41] Z. Liu, J. Wang, D. Xie, G. Chen, Small 4 (2008) 462–466.
[42] V. Abdelsayed, S. Moussa, H.M. Hassan, H.S. Aluri, M.M. Collinson, M.S. El-Shall, J. Phys. Chem. Lett. 1 (2010) 2804–2809.
[43] S. Stankovich, D.A. Dikin, R.D. Piner, K.M. Kohlhaas, A. Kleinhammes, Y. Jia, Y. Wu, S.T. Nguyen, R.S. Ruoff, Carbon 45 (2007) 1558–1565.
[44] X. Fan, W. Peng, Y. Li, X. Li, S. Wang, G. Zhang, F. Zhang, Adv. Mater. 20 (2008) 4490–4493.
[45] X. Li, Z. Si, Y. Lei, J. Tang, S. Wang, S. Su, S. Song, L. Zhao, H. Zhang, CrystEngComm 12 (2010) 2060–2063.
[46] S. Chen, R. Si, E. Taylor, J. Janzen, J. Chen, J. Phys. Chem. A 116 (2012) 12969–12976.
[47] T. Schalow, M. Laurin, B. Brandt, S. Schauermann, S. Guimond, H. Kuhlenbeck, D.E. Starr, S.K. Shaikhutdinov, J. Libuda, H. Freund, J. Angew. Chem. Int. Ed. 44 (2005) 7601–7605.
[48] J. Su, M. Cao, L. Ren, C. Hu, J. Phys. Chem. C. 115 (2011) 14469–14477.